Coexistence of symmetry-enforced phononic Dirac nodal-line net and three-nodal surfaces phonons in solid-state materials: Theory and materials realization

Jianhua Wang,[1,*] Hongkuan Yuan,[1,*] Zhi-Ming Yu,[2,3] Zeying Zhang,[4,†] and Xiaotian Wang[1,‡]

[1]*School of Physical Science and Technology, Southwest University, Chongqing 400715, China*

[2]*Beijing Key Lab of Nanophotonics & Ultrafine Optoelectronic Systems, School of Physics, Beijing Institute of Technology, Beijing, 100081, China*

[3]*Centre for Quantum Physics, Key Laboratory of Advanced Optoelectronic Quantum Architecture and Measurement (MOE), School of Physics, Beijing Institute of Technology, Beijing 100081, China*

[4]*College of Science, Beijing University of Chemical Technology, Beijing 100029, China*

(Received 23 August 2021; revised 4 November 2021; accepted 30 November 2021; published 13 December 2021)

In this study, using symmetry analysis, we reveal that symmetry-enforced three-nodal surfaces (NSs) and Dirac nodal-line (DNL) net phonons can coexist in two candidate space groups (SGs)—with SG Nos. 61 and 205—out of 230 SGs. The phononic DNL net in SGs 61 and 205 contains three phononic DNLs, which share phononic nodal point R in the momentum space and lie at the hinge between two of the three $k_i (i = x, y, z)$ planes. More interestingly, using first-principle calculations, we find that the realistic materials ZnSb (with SG No. 61) and RuS_2, P_2Pt, and OsS_2 (with SG No. 205) exhibit three NSs and DNL net phonons. In addition, we report that obvious phononic surface states can be observed in these mentioned realistic materials and will benefit their experimental detection. We hope that the proposed realistic materials can be viewed as ideal platforms to realize the DNL net and three-NSs phonons in solid-state materials.

DOI: 10.1103/PhysRevMaterials.5.124203

I. INTRODUCTION

Realistic topological semimetallic materials and their topological phenomena have been widely studied [1–7]. The electronic structures of topological semimetals are characterized by bulk band crossings, which generate gapless electronic excitations and exotic topological behaviors. Based on different dimensions of band crossings in the momentum space, topological semimetals can be divided into the following three categories: nodal-point (NP) [8–16], nodal-line (NL) [17–25], and nodal-surface (NS) semimetals [26–29] with zero-, one-, and two-dimensional band crossings in the momentum space, respectively. The NP semimetals include two- [30–32], three- [26,33–36], four- [9,10], six- [37–41], and eight- [42,43] fold degenerate NP semimetals. The NS semimetals contain one-NS, two-NSs, and three-NSs semimetals. Compared to the NP and NS semimetals, the NL semimetals have more subtypes because a line can be transformed into different geometric shapes. Moreover, the presence of more than one NL in the moment space can create rich topological states. Until now, various types of NL semimetals, such as intersecting nodal-rings [44], nodal-chains [45,46], nodal-link [47], Hopf-links [48], nodal-net [49], and nodal-knots [50] semimetals, have been proposed through first-principles calculations and symmetry analysis.

A phonon is a quantum of lattice vibrational energy and one of the most common quasiparticles for collective excitation. Phonons [51] can be studied using critical theorems and topological concepts, thus promoting the birth of topological phonons. Very recently, topological phonons in solid-state materials have become a rapidly developing new field with experimental and theoretical studies. A series of NP phonons [52–57], such as Dirac, Weyl, threefold degenerate, and sixfold degenerate phonons; NL phonons [58–63], such as nodal-chain, type III nodal-ring, intersecting nodal-ring, hourglass Weyl nodal-line, Dirac nodal-line, straight nodal-line, nodal-links, and lanternlike phonons; and NS phonons [64,65], such as one-NS and two-NSs phonons, have been predicted in realistic materials and some of them have been confirmed by experiments [66,67].

In general, the appearance of topological phonons (TPs) is closely related to the unique crystal symmetry, which is a strict structural requirement for the candidate materials. However, to the best of our knowledge, most of the previous studies [52–63] are mainly focused on the theory and materials realization of only one type of symmetry-enforced TPs; hence, symmetry analysis and materials prediction studies on (at least) two coexisting symmetry-enforced TPs are very limited. Therefore, it is necessary to determine the symmetry conditions required for the coexistence of several different types of TP states, and find a series of synthesized solid-state materials with different types of TPs. The following are the reasons: (1) Based on the symmetry conditions, in future studies, we can easily target the space groups in which different types of TP states coexist among the 230 space groups. (2) For a material with two or more types of TPs, it can be viewed as a good

*These authors contributed equally to this work.
†Corresponding author: zzy@mail.buct.edu.cn
‡Corresponding author: xiaotianwang@swu.edu.cn

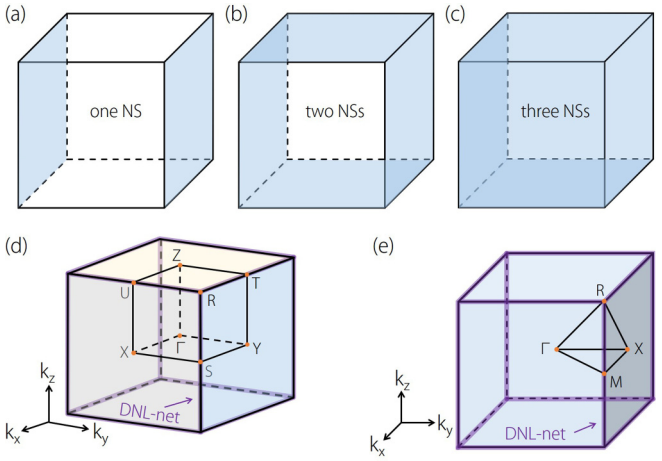

FIG. 1. (a)–(c) Schematic representations of one-NS, two-NSs, and three-NSs phonons, respectively. (d) and (e) Schematic representations of DNL net phonons in SGs 61 and 205, respectively. In (d) and (e), some symmetry points are also given.

platform to study the entanglement between these TP states. Different TP states may have different physical properties. If different types of TP states are combined into one material, unexpected physical properties may emerge.

In this study we perform a theoretical study focusing on the coexistence of symmetry-enforced three-NSs and Dirac nodal-line (DNL) net phonons. The reason for selecting this coexistence of the TP states is that until now, the three-NSs phonons, DNL net phonons, or both are still rarely investigated by researchers. By screening all the 230 space groups, we reveal that two candidate groups, with space group numbers (SG Nos.) 61 and 205, can be a good platform to search

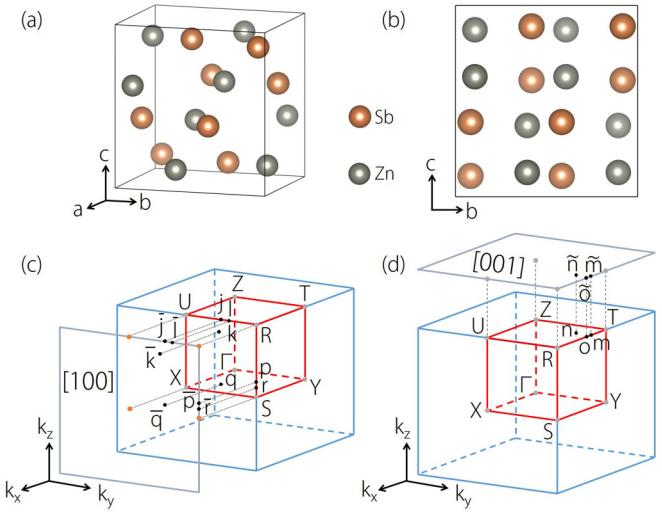

FIG. 2. (a) and (b) Primitive cell of ZnSb with *Pbca*-type structure with views of different sides. (c) and (d) Three-dimensional bulk Brillouin zone (BZ) and the [100] and [001] two-dimensional surface BZs, respectively. In (c), the $\bar{j}$, $\bar{k}$, $\bar{l}$, $\bar{p}$, $\bar{q}$ $\bar{r}$ of the [100] surface are the projections of the j, k, l, p, q, r points, respectively. In (d), the $\tilde{m}$, $\tilde{n}$, $\tilde{o}$ of the [001] surface are the projections of the m, n, o points, respectively.

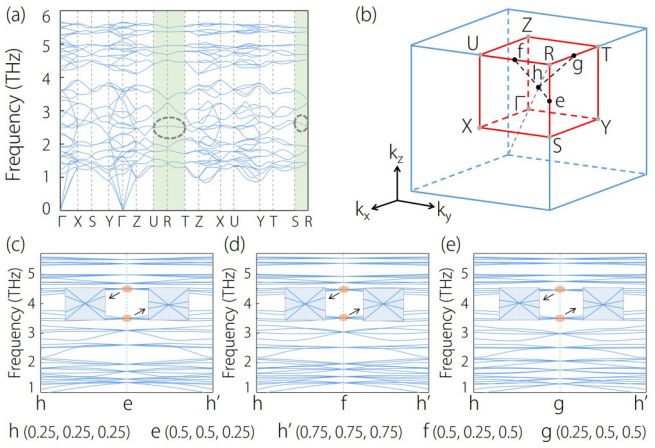

FIG. 3. (a) Phonon dispersion of ZnSb. The DNL net phonons are highlighted with a green background. (b) Three-dimensional BZ and high symmetry (U, R, T, Z, X, S, Y, Γ) and selected symmetry points (e, f, g, h). (c)–(e) Phonon dispersions of ZnSb along the h-e-h', h-f-h', and h-g-h', respectively. All the points at e, f, and g are Dirac points. For clarity, some examples are shown in the enlarged figures in (c)–(e).

for the coexistence of symmetry-enforced three-NSs and DNL net phonons. Detailed symmetry analysis is provided to prove the existence of three-NSs and DNL net phonons in SGs 61 and 205. Moreover, using the first-principles calculations, we predict that realistic materials ZnSb (with SG No. 61) [68] and RuS_2, P_2Pt, and OsS_2 (with SG No. 205) [69,70] are three-NSs phonons as well as DNL net phonons materials. The present study uncovers the possibility of the appearance of TPs with one-dimensional and two-dimensional degeneracies, that is, the coexistence of symmetry-enforced three-NSs and DNL net phonons. Moreover, it also provides a series of realistic materials that realize these two types of TPs. This systematic theoretical work can be useful for future studies (experiments and theory) investigating the coexistence of symmetry-enforced three-NSs and DNL net phonons.

In Secs. II and III we show detailed symmetry analysis to demonstrate the existence of three-NSs and DNL net phonons in SGs 61 and 205. In Secs. IV and V, a series of realistic materials samples, including ZnSb (with SG No. 61) and RuS_2, P_2Pt, and OsS_2 (with SG No. 205), are demonstrated as materials with coexisting three-NSs and DNL net phonons. Finally, the conclusions of the study are provided in Sec. VI.

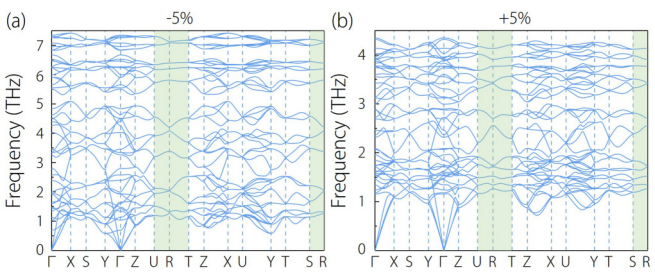

FIG. 4. (a) and (b) Phonon dispersion of ZnSb under −5% and +5% uniform strains, respectively. The DNL net phonons (with green background) were, however, maintained.

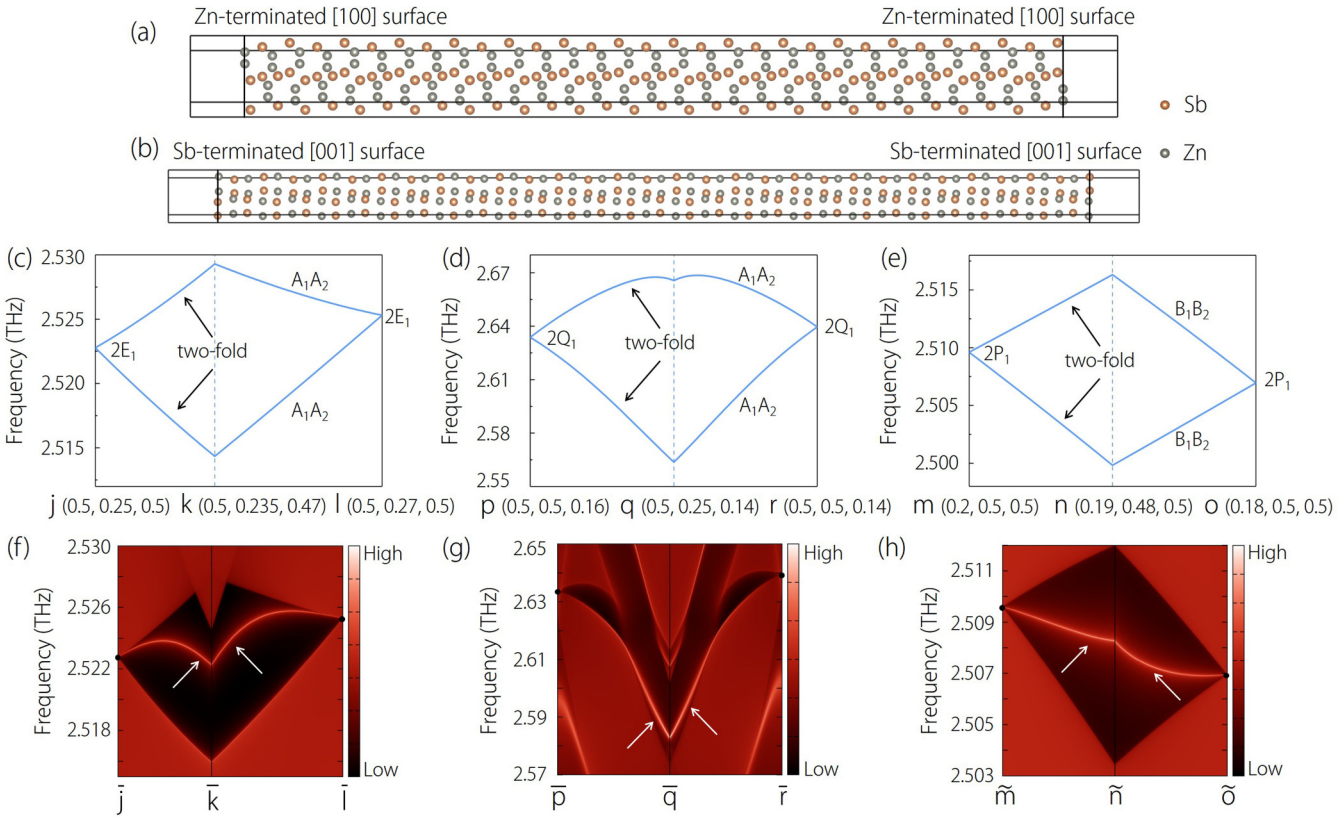

FIG. 5. (a) Atomic structure of ZnSb for Zn-terminated [100] surface. (b) Atomic structure of ZnSb for Sb-terminated [001] surface. (c)–(e) Phonon dispersions of ZnSb bulk along the j-k-l, p-q-r, and m-n-o paths, respectively. In (c)–(e), the symmetry modes for the optical branches are given. (f)–(h) Phononic surface spectra along the $\bar{j}$-$\bar{k}$-$\bar{l}$, $\bar{p}$-$\bar{q}$-$\bar{r}$, $\tilde{m}$-$\tilde{n}$-$\tilde{o}$ surface BZ on [100], [100], and [001] surfaces calculated using the iterative Greens function method based on a phononic tight-binding Hamiltonian. In (f)–(h), the black circles indicate the locations of the phonic band-crossing points, and the phononic surface states connected to the phononic band-crossing points are marked by white arrows.

II. SYMMETRY ANALYSIS OF THE THREE-NSs PHONONS IN SGs 61 AND 205

The NS, a two-dimensional twofold band degeneracy, only occurs at the boundary plane of the BZ and hosts linear dispersion in the perpendicular direction to the surface. Three possible cases of NS phonons exist, that is, the phononic systems exhibit one, two, or three NSs. The schematic illustrations of one-NS, two-NSs, and three-NSs phonons are shown in Figs. 1(a), 1(b), and 1(c), respectively. The symmetry conditions for the three-NSs phonons in SGs 61 and 205 are as follows:

Three twofold screw rotation symmetries, that is, $\{C_{2x}|\frac{1}{2}\frac{1}{2}0\}$, $\{C_{2y}|0\frac{1}{2}\frac{1}{2}\}$, and $\{C_{2z}|\frac{1}{2}0\frac{1}{2}\}$ exist in SG 61. When we consider the combination of twofold screw rotation S_2 and time-reversal symmetry $\mathcal{T}$, the phonon bands will doubly degenerate when $S_2^2 = -1$, owing to the Kramers degeneracy $(S_2\mathcal{T})^2 = -1$ (notice for spinless cases, $\mathcal{T}^2 = 1$). For example, $(\{C_{2y}|0\frac{1}{2}\frac{1}{2}\}\mathcal{T})^2 = e^{-ik_y}$ generates nodal surface in $k_y = \pi$ plane. As a result, in SG 61, there exist three-nodal surfaces at $k_x = \pi$, $k_y = \pi$, and $k_z = \pi$ planes [see Fig. 1(c)]. Similarly, there exist three twofold screw rotation operations $\{C_{2x}|\frac{1}{2}\frac{1}{2}0\}$, $\{C_{2y}|0\frac{1}{2}\frac{1}{2}\}$, and $\{C_{2z}|\frac{1}{2}0\frac{1}{2}\}$ in SG 205, and thus there should be three-nodal surfaces at $k_x = \pi$, $k_y = \pi$, and $k_z = \pi$ planes [see Fig. 1(c)].

III. SYMMETRY ANALYSIS OF THE DNL NET PHONONS IN SGs 61 AND 205

DNL net phonons contain multiple DNLs, sharing (at least) one nodal point (named as joint nodal point) in momentum space. The joint nodal point of the DNLs is located at the high-symmetry line or high-symmetry point in BZ. The DNL net phonons in SGs 61 and 205 are schematically shown in Figs. 1(d) and 1(e), respectively. The three phononic DNLs in SGs 61 and 205 share the phononic nodal point R in the momentum space and lie at the hinge between two of the three $k_i (i = x, y, z)$ planes. The symmetry conditions for the DNL net phonons in SGs 61 and 205 are as follows:

First, we consider the $E(-\frac{1}{2}k_y\frac{1}{2})$ (T-R) high-symmetry line of SG 61, and the generators of the little group of E can be selected as $g_1 = \{C_{2y}|0\frac{1}{2}\frac{1}{2}\}$ and $g_2 = \{\sigma_z|\frac{1}{2}0\frac{1}{2}\}$. g_1 and g_2 satisfy the following algebra at arbitrary point in E:

$$[g_1, g_2] = 0, \quad g_2^2 = -1. \tag{1}$$

Therefore, we can label the Bloch states at arbitrary point in E by the eigenvalues of g_2, i.e., $g_2|\pm i\rangle = \pm i|\pm i\rangle$. Consider the anticommutation relationship between g_1 and g_2, one finds that

$$g_2 g_1|\pm i\rangle = -g_1 g_2|\pm i\rangle = \mp i g_1|\pm i\rangle, \tag{2}$$

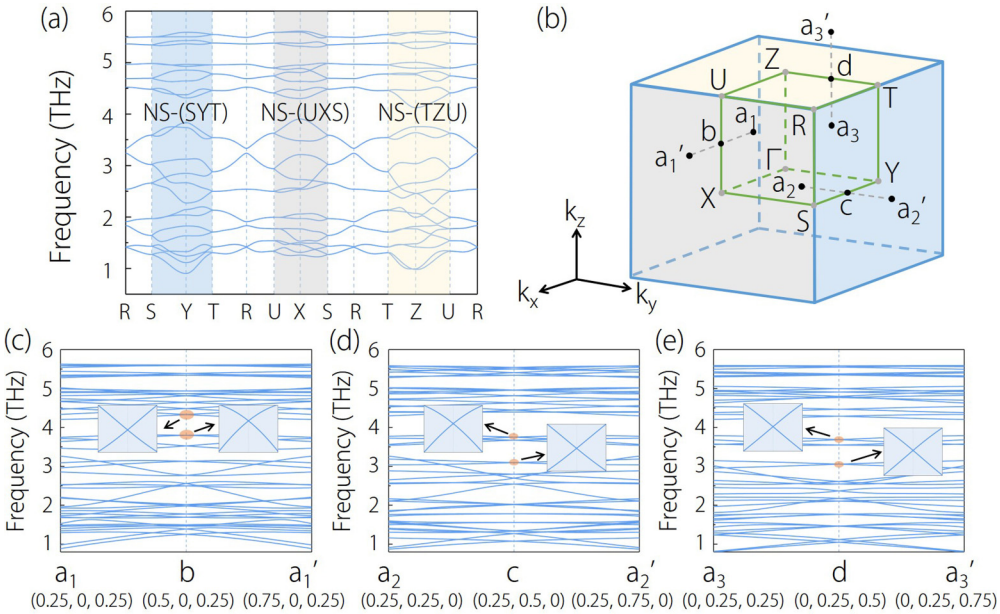

FIG. 6. (a) Phonon dispersion of ZnSb bulk along the *R*-*S*-*Y*-*T*-*R*-*U*-*X*-*S*-*R*-*T*-*Z*-*U*-*R* paths. Three NS states are highlighted with different colors. (b) Bulk BZ and some symmetry points. (c)–(e) Phonon dispersions along the a_1-b-a_1', a_2-c-a_2', and a_3-d-a_3', respectively. All the points at b, c, and d are twofold degenerate points with linear phonon bands dispersion. For clarity, some examples are shown in the enlarged figures of (c)–(e).

which indicates that there exist two pairs of degeneracies $\{|i\rangle, -ig_1|i\rangle\}$ and $\{|-i\rangle, ig_1|-i\rangle\}$. Time-reversal symmetry $\mathcal{T}$ can lead further constraints. The Bloch Hamiltonian commutes with $\mathcal{T}' = \mathcal{T}g_2$, which satisfies $\mathcal{T}'^2 = -1$, guaranteeing the Kramers degeneracy of $|\pm i\rangle$. Consequently the four states $\{|i\rangle, -ig_1|i\rangle, |-i\rangle, ig_1|-i\rangle\}$ are distinct from each other and must be degenerate in E high symmetry line.

Similarly, on the *U*-*R* high-symmetry line we use $g_1 = \{C_{2x}|\frac{1}{2}\frac{1}{2}0\}$, $g_2 = \{\sigma_z|\frac{1}{2}0\frac{1}{2}\}$, and on *S*-*R*, we use $g_1 = \{C_{2z}|\frac{1}{2}0\frac{1}{2}\}$, $g_2 = \{\sigma_y|\frac{1}{2}\frac{1}{2}0\}$. In addition, on *M*-*R* of SG 205 we use $g_1 = \{C_{2z}|\frac{1}{2}0\frac{1}{2}\}$, $g_2 = \{\sigma_x|\frac{1}{2}\frac{1}{2}0\}$. The fourfold degenerate states can also be demonstrated along the *U*-*R*, *S*-*R*, and *M*-*R* paths. Furthermore, these symmetry-enforced DNLs in SG 61 and SG 205 share the same point *R* in the momentum space and form a DNL net state.

IV. THREE-NSs AND DNL NET PHONONS IN MATERIAL WITH SG NO. 61

Here an intermetallic compound ZnSb with SG No. 61 [68] was selected as an example to demonstrate the symmetry-enforced three-NSs and DNL net phonons in its phonon dispersion. ZnSb is an existing material and its primitive cell is shown in Figs. 2(a) and 2(b). Structure relaxation of the crystal structure of ZnSb was performed using first-principles calculations, and further details on the computational methods can be found in the Supplemental Material (SM) [71]. The obtained lattice constants were $a = 6.285$ Å, $b = 7.824$ Å, and $c = 8.233$ Å, which agreed well with the experimental values of the lattice constants [68], that is, $a = 6.202$ Å, $b = 7.742$ Å, and $c = 8.100$ Å. ZnSb contains 16 atoms (i.e., eight Zn and eight Sb atoms), the Zn atoms and Sb atoms occupy the 8*c* (0.45971, 0.10641, 0.87268) and 8*c* (0.64185, 0.08268, 0.39069) Wyckoff positions, respectively. Along the symmetry paths Γ-*X*-*S*-*Y*-Γ-*Z*-*U*-*R*-*T*-*Z*-*X*-*U*-*Y*-*T*-*S*-*R* shown in Fig. 2(c), the phonon dispersion of ZnSb is shown in Fig. 3(a). ZnSb is dynamically stable owing to the absence of imaginary frequencies. As shown in Fig. 3(a), a series of fourfold degenerate phonon bands (highlighted by green backgrounds) appear along the *U*-*R*, *R*-*T*, and *S*-*R* paths. To make clear, we select three symmetry points *e*, *f*, and *g* [see Fig. 3(b)], belonging to the *S*-*R*, *U*-*R*, and *R*-*T* paths, respectively. Thereafter, we calculate the phonon dispersions along the *h*-*e*-*h*′, *h*-*f*-*h*′, and *h*-*g*-*h*′ paths, and the results are shown in Figs. 3(c)–(e). A series of phononic Dirac points, with fourfold degeneracy and linear dispersion, appear at the *e*, *f*, and *g* points. As discussed in Sec. III, these three fourfold degenerate phonon bands, which share the phononic nodal

TABLE I. Experimentally observed and calculated lattice constants for RuS_2, P_2Pt, and OsS_2 materials.

Materials	Experimental lattice constants	Calculated lattice constants
RuS_2	5.655 Å [69]	5.605 Å
P_2Pt	5.754 Å [70]	5.695 Å
OsS_2	5.664 Å [69]	5.619 Å

TABLE II. The atomic positions for the relaxed RuS_2, P_2Pt, and OsS_2, respectively.

Materials	Wyckoff positions
RuS_2	Ru 4*a* (0.5, 0, 0.5), S 8*c* (0.38720, 0.11280, 0.88720)
P_2Pt	Pt 4*a* (0.5, 0, 0.5), P 8*c* (0.38996, 0.11003, 0.88997)
OsS_2	Os 4*a*(0.5, 0, 0.5), S 8*c* (0.38407, 0.11593, 0.88407)

point R in the momentum space, actually belong to the DNL net phonons [see Fig. 1(d)]. The DNL net phonons in SG 61 belong to symmetry-enforced phonons; therefore, these DNL net phonons should be robust to the uniform strains. Figure 4 shows the phonon dispersions of ZnSb under -5% and $+5\%$ uniform strains. It can be concluded that strained ZnSb remained dynamically stable and the DNL net phonons were maintained under -5% and $+5\%$ uniform strains.

Furthermore, we study the phononic surface states of the DNL net in ZnSb. As an example, we focus on the DNL net phonons around ∼2.5 THz [see the dashed range in Fig. 3(a)]. As shown in Figs. 2(c) and 2(d) we select a series of symmetry points j, k, l m, n, o, p, q, and r. The m, n, and o points are projected to $\widetilde{m}$, $\widetilde{n}$, $\widetilde{o}$ on the [001] surface, and the j, k, l, p, q, and r points are projected to $\overline{j}$, $\overline{k}$, $\overline{l}$, $\overline{p}$, $\overline{q}$, $\overline{r}$ on the [100] surface. We select Zn-terminated [100] surface and Sb-terminated [001] surface to calculate the surface state [see the atomic structures in Figs. 5(a) and 5(b)]. The phonon dispersions of ZnSb bulk along the j-k-l, p-q-r, and m-n-o paths are shown in Figs. 5(c)–5(e) as references. It can be seen that the phononic Dirac points appear at the j, l, p, r, m, and o points. The phononic surface spectra on the [100] and [001] surfaces were calculated using two different methods, that is, using the iterative Greens function method based on a phononic tight-binding Hamiltonian [Figs. 5(f)–5(h)], and by constructing a slab model based on ZnSb [Figs. S4(a)–S4(c)]. In Figs. 5(f)–5(h) it can be seen that the phononic surface states (represented by arrows) are connected to the DNL net. To understand the possibility of finding the connected phononic surface states for the DNL net at other frequencies, we examined the phononic surface spectra of the DNL net around ∼3.1 THz, shown in Figs. S1–S3 of the SM [71]. Similarly, the phononic surface states, arising from the phononic band-crossing points, can be obviously seen on the [100] and [001] surfaces.

We have calculated the phonon modes for the phonon dispersions [see Figs. 5(c)–5(e)], The phonon modes are labeled in Γ notation and are obtained by the SpaceGroupIrep code [72,73]. We define the $k_x = \pi$ plane as A and $k_z = \pi$ plane as B in space group 61. Then the optical modes at A plane around 2.5 THz contains A_1A_2 twice, where A_1A_2 are two one-dimensional irreducible representations that conjugate to each other. On high symmetry line U-R (E), the optical mode is formed by two two-dimensional irreducible representation E_1 which is stuck together by time-reversal symmetry. The phonon modes are consistent with the symmetry analysis results in Sec. II.

As shown in Fig. 6(a), all the phonon bands along the S-Y-T, U-X-S, and T-Z-U paths contain twofold degeneracy. For clarity we selected some symmetry lines, i.e., a_1-b-a_1', a_2-c-a_2', and a_3-d-a_3' [see Fig. 6(b)], which are perpendicular to the U-X, S-Y, and Z-T symmetry lines, respectively. Thereafter, we calculated phonon dispersions along the a_1-b-a_1', a_2-c-a_2', and a_3-d-a_3', paths, and the results are shown in Figs. 6(c)–6(e). It can be clearly seen that a series of twofold degenerate points at b, c, and d symmetry points with linear band dispersion exist. As discussed in Sec. II, the twofold degenerate phonon bands along the S-Y-T, U-X-S, and T-Z-U paths can form three-NSs phonons. Moreover, as discussed in Secs. II and III, the DNL net and three-NSs phonons in ZnSb belong to symmetry-enforced nodal structures. Hence, these two types of phonons should be observed in other material samples with SG No. 61.

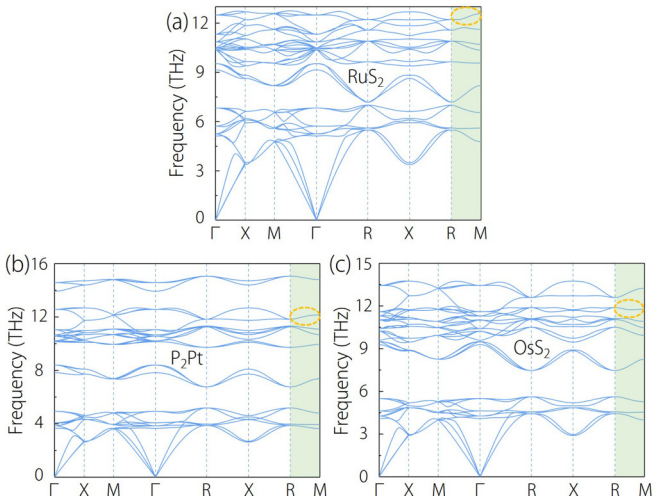

FIG. 7. (a)–(c) Phonon dispersions of RuS_2, P_2Pt, and OsS_2 with the $Pa\bar{3}$-type structure. The DNL net states are highlighted with a green background.

V. THREE-NSs AND DNL NET PHONONS IN MATERIALS WITH SG NO. 205

Herein we study some realistic materials with SG No. 205 as the candidates to realize the coexistence of the DNL net and three-NSs phonons. As shown in Figs. S5(a)–S5(c), the RuS_2, P_2Pt, and OsS_2 materials [69,70] with the $Pa\bar{3}$-type structure were selected as targets, and the primitive cells of these compounds are shown in the figure. Dahl [70] prepared a P_2Pt alloy by mixing 70% of platinum metal powder and 30% of red phosphorus and heating for three weeks in an evacuated and sealed silica tube at ∼570 °C. Sutarno *et al.* [69] obtained RuS_2 by heating Ru_9S_8 and sulfur overnight at 950 °C and cooling in a furnace. Moreover, OsS_2 had been synthesized for a detailed x-ray diffraction study of the compound [69]. The experimentally obtained and calculated lattice constants for these three materials are listed in Table I. It can be seen that the calculated values agree well with the experimental ones [69,70]. The atomic positions for the relaxed RuS_2, P_2Pt, and OsS_2 are given in Table II.

Along the Γ-X-M-Γ-R-X-R-M paths [Fig. S5(d)], the phonon dispersions of RuS_2, P_2Pt, and OsS_2 with the $Pa\bar{3}$-type structure are shown in Figs. 7(a)–7(c). It can be seen that the phonon bands along the R-M path contain fourfold degeneracy. Based on the discussion in Sec. III, the phonon bands along the R-M can form DNL net phonons in the momentum space, as shown in Fig. S5(d). We select S and Ru-terminated [001] surfaces to calculate the surface states [see Fig. 8(a)]. To examine the phononic surface spectra of these materials, in Figs. 8(b), S6(a), and S6(b), we selected some phonon band-crossing points, such as M_1', M_2', M_3', X_1', X_2', X_3', R_1, R_2, R_3, and these points were projected to $\widetilde{M}_1'$, $\widetilde{M}_2'$, $\widetilde{M}_3'$, $\widetilde{X}_1'$, $\widetilde{X}_2'$, $\widetilde{X}_3'$, $\widetilde{R}_1$, $\widetilde{R}_2$, $\widetilde{R}_3$ on the [001] surface. The phononic surface spectra of RuS_2, P_2Pt, and OsS_2 along the

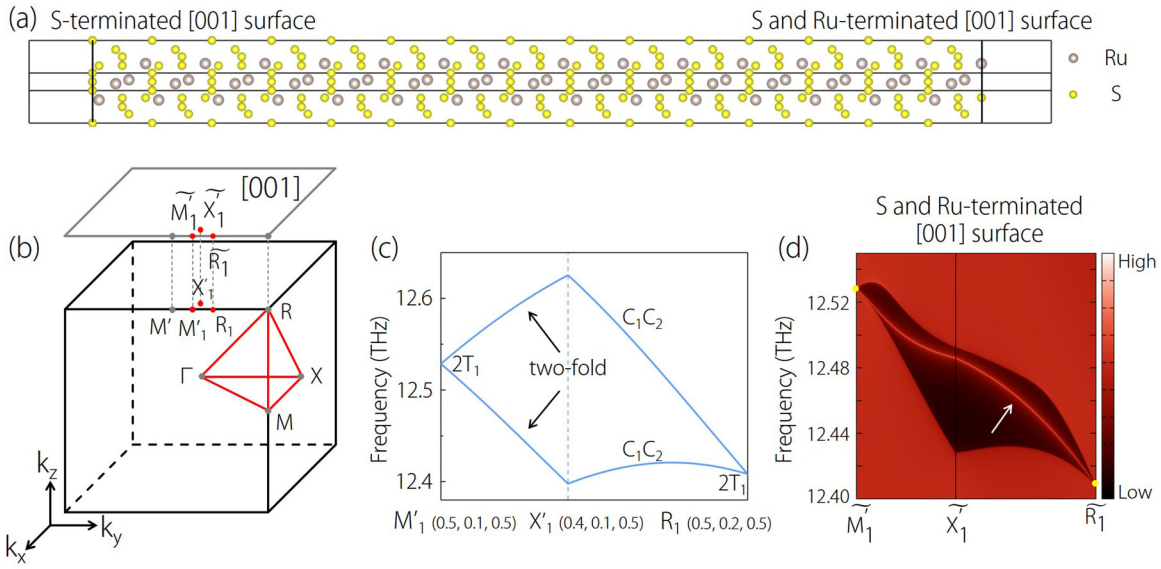

FIG. 8. (a) Atomic structure of RuS_2 for S-terminated [001] surface, and S and Ru-terminated [001] surface. (b) Three-dimensional bulk BZ and [001] two-dimensional surface BZ. Some symmetry points M_1', X_1', R_1 are selected in the three-dimensional BZ and are projected to $\widetilde{M}_1'$, $\widetilde{X}_1'$, $\widetilde{R}_1$ on the [001] surface. (c) Phonon dispersions of RuS_2 bulks along the M_1'-X_1'-R_1, paths, respectively. In (c), the symmetry modes for the optical branches are given. (d) S and Ru-terminated [001] surface states, along the $\widetilde{M}_1'$-$\widetilde{X}_1'$-$\widetilde{R}_1$ paths, calculated using the iterative Greens function method based on a phononic tight-binding Hamiltonian.

$\widetilde{M}_1'$-$\widetilde{X}_1'$-$\widetilde{R}_1$, $\widetilde{M}_2'$-$\widetilde{X}_2'$-$\widetilde{R}_2$, $\widetilde{M}_3'$-$\widetilde{X}_3'$-$\widetilde{R}_3$ paths are shown in Figs. 8(d), S6(e), and S6(f), respectively. As a reference, the phonon dispersions of RuS_2, P_2Pt, and OsS_2 bulks along the M_1'-X_1'-R_1, M_2'-X_2'-R_2, and M_3'-X_3'-R_3 paths are shown in Figs. 8(c), S6(c), and S6(d). The phononic surface states occur from the phonon band-crossing points, and these states are represented by white arrows in Figs. 8(d), S6(e), and S6(f).

Figures 9(a)–9(c) show the phonon dispersions of RuS_2, P_2Pt, and OsS_2 along the M-X-R paths, respectively. All the phonon bands along the M-X-R paths contain twofold degeneracy. Based on the discussion in Sec. II, the two phonon bands degenerate in the entire $k_i (i = x, y, z)$ planes, creating three-NSs phonons [Fig. 1(c)]. One important feature of the NS phonons is that they host linear dispersion along the

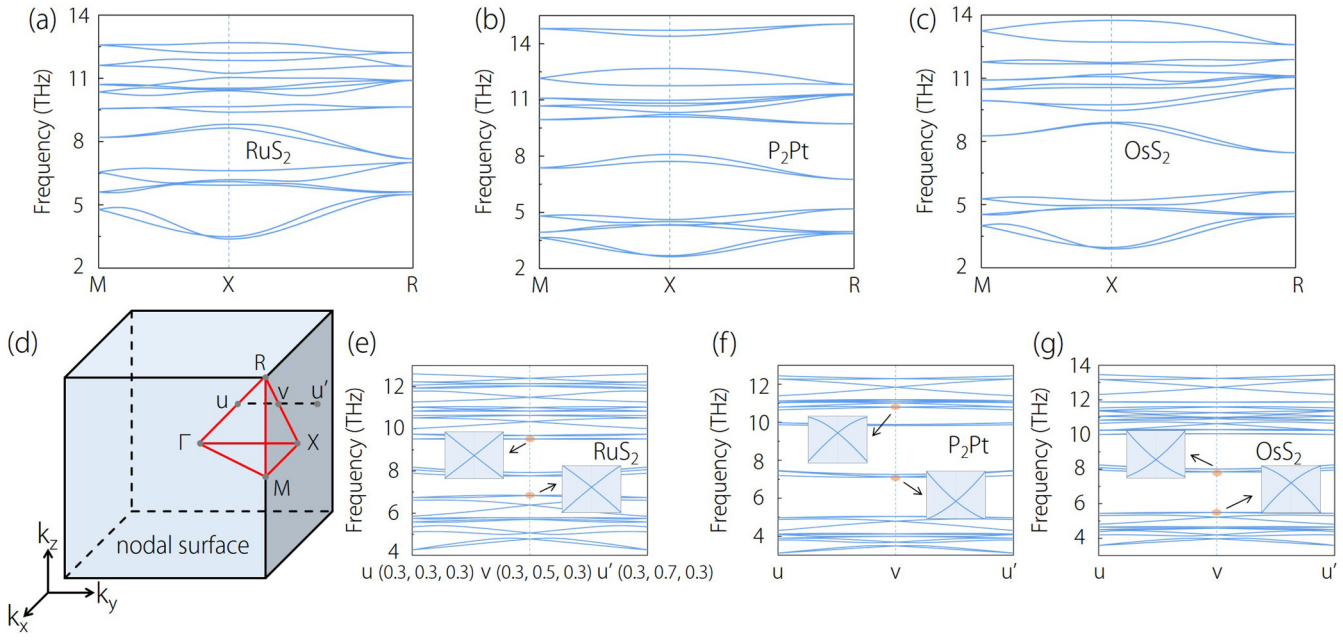

FIG. 9. (a)–(c) Phonon dispersions of RuS_2, P_2Pt, and OsS_2 along the M-X-R paths, respectively. (d) Bulk BZ and some selected symmetry points. The NS phonons appear on the $k_i (i = x, y, z)$ planes. (e)–(g) Phonon dispersions of RuS_2, P_2Pt, and OsS_2 along the u-v-u' paths, respectively. All the points at v are twofold degenerate points with linear phonon bands dispersion. For clarity, some examples are shown in the enlarged figures in (e)–(g).

surface normal [26]. As shown in Fig. 9(d), we selected a symmetry path u-v-u' normal to the $k_y = \pi$ plane. The phonon dispersions of RuS_2, P_2Pt, and OsS_2 along the u-v-u' paths are shown in Figs. 9(e)–9(g), respectively. All the phonon band-crossing points at v are two-degenerate points with linear dispersion [see the examples in the enlarged figures in Figs. 9(e)–(g)].

VI. CONCLUSIONS

To summarize, we demonstrated the coexistence of DNL net and three-NSs phonons in SGs 61 and 205 of 230 SGs, using first-principles calculations and symmetry analysis. Moreover, we proposed that the realistic materials ZnSb (with SG No. 61) and RuS_2, P_2Pt, and OsS_2 (with SG No. 205) exhibit three-NSs and DNL net phonons. The obvious phononic surface states on the [100] and [001] surfaces BZ will benefit for the experimental confirmation. The proposed coexistence of the DNL net and three-NSs phonon states in SGs 61 and 205 belong to the symmetry-enforced phonon states; therefore, the materials with SGs 61 and 205 must host the coexistence of DNL net and three-NSs at their phonon dispersions. Our results not only uncover a class of symmetry-enforced coexistence phonon states, i.e., DNL net and three-NSs phonons, but also provide an effective method to search for the coexistence of DNL net and three-NSs phonon states in solid-state materials.

ACKNOWLEDGMENTS

Z.Z. is grateful for the support from the National Natural Science Foundation of China (Grant No. 12004028). X.W. is grateful for the support from the National Natural Science Foundation of China (No. 51801163) and the Natural Science Foundation of Chongqing (No. cstc2018jcyjA0765).

[1] A. A. Burkov, Nat. Mater. **15**, 1145 (2016).
[2] B. Q. Lv, T. Qian, and H. Ding, Rev. Mod. Phys. **93**, 025002 (2021).
[3] J. Hu, S.-Y. Xu, N. Ni, and Z. Mao, Annu. Rev. Mater. Res. **49**, 207 (2019).
[4] B. Yan and C. Felser, Annu. Rev. Condens. Matter Phys. **8**, 337 (2017).
[5] F. Tang, H. C. Po, A. Vishwanath, and X. Wan, Nature (London) **566**, 486 (2019).
[6] Y. Xu, L. Elcoro, Z. D. Song, B. J. Wieder, M. G. Vergniory, N. Regnault, Y. L. Chen, C. Felser, and B. A. Bernevig, Nature (London) **586**, 702 (2020).
[7] Z.-M. Yu, Z. Zhang, G.-B. Liu, W. Wu, X.-P. Li, R.-W. Zhang, S. A. Yang, and Y. Yao, Sci. Bull. (2021), doi: 10.1016/j.scib.2021.10.023.
[8] Z. Zhu, Z.-M. Yu, W. Wu, L. Zhang, W. Zhang, F. Zhang, and S. A. Yang, Phys. Rev. B **100**, 161401(R) (2019).
[9] Q. D. Gibson, L. M. Schoop, L. Muechler, L. S. Xie, M. Hirschberger, N. P. Ong, R. Car, and R. J. Cava, Phys. Rev. B **91**, 205128 (2015).
[10] S. M. Young and C. L. Kane, Phys. Rev. Lett. **115**, 126803 (2015).
[11] N. P. Armitage, E. J. Mele, and A. Vishwanath, Rev. Mod. Phys. **90**, 015001 (2018).
[12] B. J. Yang and N. Nagaosa, Nat. Commun. **5**, 4898 (2014).
[13] B. J. Wieder, Y. Kim, A. M. Rappe, and C. L. Kane, Phys. Rev. Lett. **116**, 186402 (2016).
[14] A. A. Soluyanov, D. Gresch, Z. Wang, Q. Wu, M. Troyer, X. Dai, and B. A. Bernevig, Nature (London) **527**, 495 (2015).
[15] H.-X. Wang, Z.-K. Lin, B. Jiang, G.-Y. Guo, and J.-H. Jiang, Phys. Rev. Lett. **125**, 146401 (2020).
[16] L. Tian, Y. Liu, W. W. Yu, X. M. Zhang, and G. D. Liu, Phys. Rev. B **104**, 045137 (2021).
[17] C. Fang, Y. Chen, H.-Y. Kee, and L. Fu, Phys. Rev. B **92**, 081201(R) (2015).
[18] S.-Y. Yang, H. Yang, E. Derunova, S. S. P. Parkin, B. Yan, and M. N. Ali, Adv. Phys. X **3**, 1414631 (2018).
[19] G. Bian, T.-R. Chang, R. Sankar, S.-Y. Xu, H. Zheng, T. Neupert, C.-K. Chiu, S.-M. Huang, G. Chang, I. Belopolski, D. S. Sanchez, M. Neupane, N. Alidoust, C. Liu, B. Wang, H.-T. Jeng, A. Bansil, F. Chou, H. Lin, and M. Z. Hasan, Nat. Commun. **7**, 10556 (2016).
[20] A. Lau, T. Hyart, C. Autieri, A. Chen, and D. I. Pikulin, Phys. Rev. X **11**, 031017 (2021).
[21] R. Takahashi, M. Hirayama, and S. Murakami, Phys. Rev. B **96**, 155206 (2017).
[22] C. Fang, H. Weng, X. Dai, and Z. Fang, Chin. Phys. B **25**, 117106 (2016).
[23] Z. M. Yu, W. Wu, X. L. Sheng, Y. X. Zhao, and S. A. Yang, Phys. Rev. B **99**, 121106(R) (2019).
[24] X. P. Li, B. Fu, D. S. Ma, C. Cui, Z. M. Yu, and Y. Yao, Phys. Rev. B **103**, L161109 (2021).
[25] K. Wang, J.-X. Dai, L. B. Shao, S. A. Yang, and Y. X. Zhao, Phys. Rev. Lett. **125**, 126403 (2020).
[26] W. Wu, Y. Liu, S. Li, C. Zhong, Z.-M. Yu, X.-L. Sheng, Y. X. Zhao, and S. A. Yang, Phys. Rev. B **97**, 115125 (2018).
[27] S. Z. Chen, S. Li, Y. Chen, and W. Duan, Nano Lett. **20**, 5400 (2020).
[28] B.-B. Fu, C.-J. Yi, T.-T. Zhang, M. Caputo, J.-Z. Ma, X. Gao, B. Q. Lv, L.-Y. Kong, Y.-B. Huang, P. Richard, M. Shi, V. N. Strocov, C. Fang, H.-M. Weng, Y.-G. Shi, T. Qian, and H. Ding, Sci. Adv. **5**, eaau6459 (2019).
[29] Q.-F. Liang, J. Zhou, R. Yu, Z. Wang, and H. Weng, Phys. Rev. B **93**, 085427 (2016).
[30] C. X. Cui, X.-P. Li, D.-S. Ma, Z.-M. Yu, and Y. G. Yao, Phys. Rev. B **104**, 075115 (2021).
[31] S. Jia, S.-Y. Xu, and M. Z. Hasan, Nat. Mater. **15**, 1140 (2016).
[32] B. Q. Lv, H. M. Weng, B. B. Fu, X. P. Wang, H. Miao, J. Ma, P. Richard, X. C. Huang, L. X. Zhao, G. F. Chen, Z. Fang, X. Dai, T. Qian, and H. Ding, Phys. Rev. X **5**, 031013 (2015).
[33] J. H. Park, J. M. Coy, T. S. Kasirga, C. Huang, Z. Fei, S. Hunter, and D. H. Cobden, Nature (London) **500**, 431 (2013).
[34] Z. Zhu, G. W. Winkler, Q. S. Wu, J. Li, and A. A. Soluyanov, Phys. Rev. X **6**, 031003 (2016).
[35] Y. Xia and G. Li, Phys. Rev. B **96**, 241204(R) (2017).
[36] J. Krempaský, L. Nicolaï, M. Gmitra, H. Chen, M. Fanciulli, E. B. Guedes, M. Caputo, M. Radović, V. V. Volobuev, O. Caha,

G. Springholz, J. Minár, and J. H. Dil, Phys. Rev. Lett. **126**, 206403 (2021).
[37] C. K. Barman, C. Mondal, S. Pujari, B. Pathak, and A. Alam, Phys. Rev. B **102**, 155147 (2020).
[38] S. Nie, B. A. Bernevig, and Z. Wang, Phys. Rev. Res. **3**, L012028 (2021).
[39] L. Jin, Y. Liu, X. Zhang, X. Dai, and G. Liu, Phys. Rev. B **104**, 045111 (2021).
[40] Z. P. Sun, C. Q. Hua, X. L. Liu, Z. T. Liu, M. Ye, S. Qiao, Z. H. Liu, J. S. Liu, Y. F. Guo, Y. H. Lu, and D. W. Shen, Phys. Rev. B **101**, 155114 (2020).
[41] N. Kumar, M. Yao, J. Nayak, M. G. Vergniory, J. Bannies, Z. Wang, N. B. M. Schröter, V. N. Strocov, L. Müchler, W. Shi, E. D. L. Rienks, J. L. Mañes, C. Shekhar, S. S. P. Parkin, J. Fink, G. H. Fecher, Y. Sun, B. A. Bernevig, and C. Felser, Adv. Mater. **32**, 1906046 (2020).
[42] J. Cano, B. Bradlyn, and M. G. Vergniory, APL Mater. **7**, 101125 (2019).
[43] B. Bradlyn, J. Cano, Z. Wang, M. G. Vergniory, C. Felser, R. J. Cava, and B. A. Bernevig, Science **353**, 5037 (2016).
[44] C. Gong, Y. Xie, Y. Chen, H.-S. Kim, and D. Vanderbilt, Phys. Rev. Lett. **120**, 106403 (2018).
[45] T. Bzdušek, Q. S. Wu, A. Rüegg, M. Sigrist, and A. A. Soluyanov, Nature (London) **538**, 75 (2016).
[46] S. S. Wang, Y. Liu, Z. M. Yu, X. L. Sheng, and S. A. Yang, Nat. Commun. **8**, 1844 (2017).
[47] Z. Yan, R. Bi, H. Shen, L. Lu, S.-C. Zhang, and Z. Wang, Phys. Rev. B **96**, 041103(R) (2017).
[48] G. Chang, S.-Y. Xu, X. Zhou, S.-M. Huang, B. Singh, B. Wang, I. Belopolski, J. Yin, S. Zhang, A. Bansil, H. Lin, and M. Z. Hasan, Phys. Rev. Lett. **119**, 156401 (2017).
[49] J.-T. Wang, S. Nie, H. Weng, Y. Kawazoe, and C. Chen, Phys. Rev. Lett. **120**, 026402 (2018).
[50] R. Bi, Z. Yan, L. Lu, and Z. Wang, Phys. Rev. B **96**, 201305(R) (2017).
[51] Y. Liu, X. Chen, and Y. Xu, Adv. Funct. Mater. **30**, 1904784 (2020).
[52] Z. J. Chen, R. Wang, B. W. Xia, B. B. Zheng, Y. J. Jin, Y. J. Zhao, and H. Xu, Phys. Rev. Lett. **126**, 185301 (2021).
[53] T. Zhang, Z. Song, A. Alexandradinata, H. Weng, C. Fang, L. Lu, and Z. Fang, Phys. Rev. Lett. **120**, 016401 (2018).
[54] B. W. Xia, R. Wang, Z. J. Chen, Y. J. Zhao, and H. Xu, Phys. Rev. Lett. **123**, 065501 (2019).
[55] Q.-B. Liu, Z. Wang, and H.-H. Fu, Phys. Rev. B **103**, L161303 (2021).
[56] S. Singh, Q. S. Wu, C. Yue, A. H. Romero, and A. A. Soluyanov, Phys. Rev. Mater. **2**, 114204 (2018).
[57] C. W. Xie, Y. Liu, Z. Y. Zhang, F. Zhou, T. Yang, M. Q. Kuang, X. T. Wang, and G. Zhang, Phys. Rev. B **104**, 045148 (2021).
[58] G. Liu, Y. J. Jin, Z. J. Chen, and H. Xu, Phys. Rev. B **104**, 024304 (2021).
[59] J. J. Zhu, W.-K. Wei, J. Z. Zhao, H. Chen, L. F. Zhang, and S. A. Yang, arXiv:2104.14816.
[60] Q.-B. Liu, H.-H. Fu, and R. Q. Wu, Phys. Rev. B **104**, 045409 (2021).
[61] J. Li, J. Liu, S. A. Baronett, M. Liu, L. Wang, and R. Li, Y. Chen, D. Li, Q. Zhu, and X.-Q. Chen, Nat. Commun. **12**, 1204 (2021).
[62] B. B. Zheng, F. Y. Zhan, X. Z. Wu, R. Wang, and J. Fan, Phys. Rev. B **104**, L060301 (2021).
[63] B. Zheng, B. Xia, R. Wang, Z. Chen, J. Zhao, Y. Zhao, and H. Xu, Phys. Rev. B **101**, 100303(R) (2020).
[64] Q.-B. Liu, Z.-Q. Wang, and H.-H. Fu, Phys. Rev. B **104**, L041405 (2021).
[65] X. Wang, F. Zhou, T. Yang, M. Kuang, Z.-M. Yu, and G. Zhang, Phys. Rev. B **104**, L041104 (2021).
[66] H. Miao, T. T. Zhang, L. Wang, D. Meyers, A. H. Said, Y. L. Wang, Y. G. Shi, H. M. Weng, Z. Fang, and M. P. M. Dean, Phys. Rev. Lett. **121**, 035302 (2018).
[67] T. T. Zhang, H. Miao, Q. Wang, J. Q. Lin, Y. Cao, G. Fabbris, A. H. Said, X. Liu, H. C. Lei, Z. Fang, H. M. Weng, and M. P. M. Dean, Phys. Rev. Lett. **123**, 245302 (2019).
[68] F. L. Carter and R. Mazelsky, J. Phys. Chem. Solids **25**, 571 (1964).
[69] H. Sutarno, O. Knop, and I. G. Reid, Can. J. Chem. **45**, 1391 (1967).
[70] E. Dahl, Acta Chem. Scand. **23**, 2677 (1969).
[71] See Supplemental Material at http://link.aps.org/supplemental/10.1103/PhysRevMaterials.5.124203 for computational methods, the three-dimensional bulk BZ and two-dimensional [001] and [001] surfaces, the phonon dispersions of ZnSb bulk, and the phononic surface spectra on the [100] and [001] surfaces connected to the DNL net at around ∼3.1 THz, primitive cells of RuS_2, P_2Pt, and OsS_2, and the phononic surface spectra of P_2Pt, and OsS_2.
[72] G.-B. Liu, M. Chu, Z. Zhang, Z.-M. Yu, and Y. Yao, Comput. Phys. Commun. **265**, 107993 (2021).
[73] C. Bradley and A. Cracknell, *The Mathematical Theory of Symmetry in Solids: Representation Theory for Point Groups and Space Groups* (Oxford University Press, Oxford, 2009).